Gating of Nanopores: Modeling and Implementation of Logic Gates

Salvador Mafe,[†] José A. Manzanares,[†] and Patricio Ramirez*[,‡]

Departament de Física de la Terra i Termodinàmica, Universitat de València, E-46100 Burjassot, Spain, and Department de Física Aplicada, Universidad Politécnica de Valencia, E-46022 Valencia, Spain

Received: September 13, 2010; Revised Manuscript Received: October 16, 2010

Nanoporous and nanofluidic structures can be coated with metal and insulating layers deposited on the pore surface: when an electrolyte solution is in contact with the internal insulating layer, well-defined ionic conductance levels could be tuned by applying a gate potential to the external metallic layer. We study theoretically the dependence of the effective gate potential at the insulating layer/solution interface with the applied gate potential at the metallic surface as well as the change of the nanopore conductance with the gate potential for different electrolyte solution concentrations and nanopore radii. We solve the Poisson−Boltzmann equation to obtain the electrical potential distribution in the two regions of the pore cross-section, the insulating layer, and the inner pore solution. The model provides estimations of the effective nanopore surface charge density that could be achieved by gating the nanopore (this charge determines the nanopore selectivity in practical cases). As an application, we have shown that *NOR* and *NAND* logic gate schemes based on input and output electrical signals could be implemented by exploiting the gating of the nanopore conductance.

Introduction

Nanopores,[1−7] nanoelectrodes,[7−9] and nanopipettes[10,11] constitute a new generation of devices designed for single-molecule sensing and separation. Nanostructures based on asymmetric pores with only one type of electric charge, bipolar diodes, and transistors composed by regions of different charge juxtaposed in series and nanofluidic diodes with amphoteric chains functionalized on the pore surface have been reported.[12−15] Most previous studies concern fundamental research on the nanostructure characteristics, with emphasis on the ionic selectivity and rectification properties. These properties are usually based on the nanopore fixed charges and nanostructure asymmetry. However, practical applications will require both the design of applied schemes based on the nanostructure characteristics and the study of new experimental methods to tune the nanopore selectivity and conductance.

Most studies with nanometer-scaled pores concern molecular separation and sensing applications[2,5,7,8,10,11,16−18] and involve only a single nanopore element such as a diode or transistor. Ionic devices are intrinsically slower compared to electronic systems, but potential applications should appear in areas in which electronic diodes and transistors cannot be used. Biomolecules such as DNA and proteins function in a water environment; thus building sensors for them requires operating in a solution as well. This involves typically detecting very small signals so that ionic amplifiers would be very helpful and could potentially increase the detection limit. Ionic circuits could be used for manipulating, switching, redirecting, and amplifying biomolecules and ions in a solution.

To date, almost no logic nanodevices have been demonstrated despite the fact that biological ion channels with pH-dependent fixed charges are known to be responsible for information processing in biophysical structures.[19] We have demonstrated theoretically and experimentally that single-track conical nanopores functionalized with polyprotic acid chains show three levels of conductance that can be tuned externally (because of the pH-sensitive fixed charges) and proposed a logic gate scheme where binary and multivalued logical functions were implemented using chemical and electrical inputs.[20] (Other recent proposals for logical gates involving chemical concepts can be found elsewhere.[21−25]) Integration of microchannels and nanopores in chip-based ionic circuits[24,25] should allow faster system responses and could be useful for analytical applications involving information processing. A nanoporous system with electrically addressable element would be an ideal component of ionic circuit.

Indeed, recent theoretical and experimental studies have addressed the possibility of tuning the nanopore conductance by using a layer of a dielectric film deposited on a metallic surface inside the pore. When an electrolyte solution is in contact with this insulating layer, well-defined ionic conductance levels could be externally tuned by a gate potential applied directly to the external metallic surface.[26−30] However, the fact is that the experimental effects observed are only partly understood.[29−31] The efficiency of the conductance modulation depends on the relationship between the *effective* gating potential obtained at the insulating surface in contact with the inner electrolyte solution and the *applied* gate potential at the metallic surface. In particular, the modulation efficiency relies on the effective surface charge density,[32] which dictates the change of the nanopore conductance ΔG with the gate potential. We propose to address the above questions in this paper.

The tuning of the nanopore conductance with the gate potential could be exploited in sensing applications[5,7,10,11] and logic gate schemes similar to those implemented previously using chemical inputs.[20] To this end, we have studied first the dependence of the nanopore conductance G with the applied gate potential for different electrolyte concentrations and nanopore radii using the Poisson−Boltzmann equation. From the electrical potential distribution obtained for the two regions (the insulating layer and the inner pore solution) of the pore cross-section, we can give estimations of the effective nanopore

* Corresponding Author, E-mail: patraho@fis.upv.es.
[†] Universitat de València.
[‡] Universidad Politécnica de Valencia.

10.1021/jp1087114
Published on Web 11/10/2010

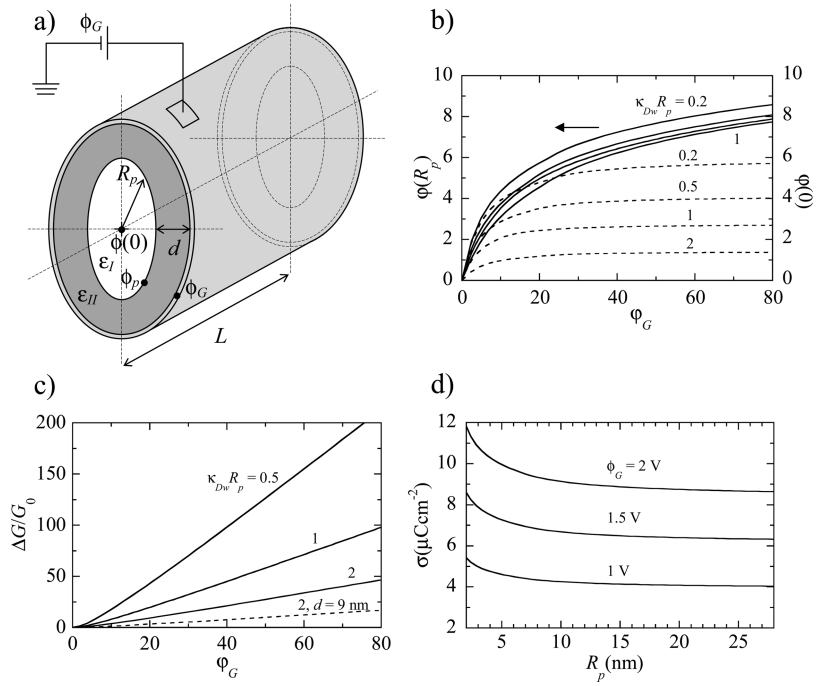

Figure 1. Scheme of the nanopore of radius R_p. The applied $\phi_G \equiv \phi(R_p + d)$ and effective $\phi_p \equiv \phi(R_p)$ gate potentials at the two ends of the insulating region of thickness d are shown (a). The (dimensionless) effective gate potential $\varphi_p \equiv \varphi(R_p)$ and the (dimensionless) potential at the pore center $\varphi(0)$ vs the (dimensionless) applied gate potential φ_G ($\varphi_G = 40$ corresponds to 1 V approximately). The numbers on the curves are the ratios between the pore radius and the Debye length (b). The relative changes $\Delta G/G_0$ of the nanopore conductance vs φ_G for different ratios between the pore radius and the Debye length (the discontinuous curve has been obtained with $d = 9$ nm instead of $d = 3$ nm in the continuous curves) (c). The effective surface charge density σ vs R_P for different gate potentials at $c_0 = 1$ mM (d).

surface charge density that could be achieved by gating the nanopore (this charge determines the nanopore selectivity in practical cases). Second, we have demonstrated theoretically *NOR* and *NAND* logic gate schemes based on the gating of the nanopore conductance (the *NAND* gate is one of the two basic logic gates, along with the *NOR* gate, from which any other logic gates can be built; because of this property, *NAND* and *NOR* gates are the *universal gates*). These results should be of conceptual interest in view of the broad list of chemically and electrochemically switchable nanopores that have been reported[5,7,10,12−18,20,26−30] and can also guide experimentalists to build logic ionic circuits.

Model

Figure 1a shows a scheme of the cylindrical nanopore (extensions to other geometries, e.g., conical or biconical nanopores, should be possible by introducing the nanopore radius dependence on the axial position; the gate voltage is applied on the metallic, equipotential surface and it does not change along the nanopore). The radius of the inner pore region, filled with a 1:1 electrolyte, is R_p. The applied and effective gate potentials at the outer and inner boundaries of the insulating region of thickness d are $\phi_G \equiv \phi(R_p + d)$ and $\phi_p \equiv \phi(R_p)$, respectively. Despite the nanometer scales involved in the problem, continuum theories[1,3,7,13−17,20,26−35] can predict correctly the observed behavior. The Poisson−Boltzmann (P−B) equation describing the radial potential distribution in the inner pore solution (region I of Figure 1a) is

$$\frac{d^2\phi}{dr^2} + \frac{1}{r}\frac{d\phi}{dr} = \frac{2Fc_0}{\varepsilon_I}\sinh\frac{F\phi}{RT} \qquad (1)$$

where r is the radial coordinate, $\phi(r)$ is the electric potential, F and R are the Faraday and universal gas constants, T is the absolute temperature, and ε_I is the solution electrical permittivity, which is that of water approximately. The origin of electrical potential is taken outside the pore, where the electrolyte concentration is c_0. By introduction of the dimensionless potential $\varphi \equiv F\phi/RT$ and the reciprocal Debye length $\kappa_{Dw} \equiv (2F^2c_0/\varepsilon_I RT)^{1/2}$, eq 1 transforms to

$$\frac{1}{r}\frac{d}{dr}\left(r\frac{d\varphi}{dr}\right) = \kappa_{Dw}^2 \sinh\varphi \qquad (2)$$

The boundary condition at $r = 0$ is

$$\left(\frac{d\varphi}{dr}\right)_0 = 0 \qquad (3)$$

and the effective surface charge density at $r = R_p$ can be obtained from the Gauss theorem as

$$\sigma = \frac{\varepsilon_I RT}{F}\left(\frac{d\varphi}{dr}\right)_{R_p-} \qquad (4)$$

The continuity of the electrical displacement vector at the pore/insulating layer interface gives

$$\varepsilon_I\left(\frac{d\varphi}{dr}\right)_{R_p-} = \varepsilon_{II}\left(\frac{d\varphi}{dr}\right)_{R_p+} \qquad (5)$$

where ϵ_{II} is the electrical permittivity of the insulating layer. The P−B equation in the insulating layer (region II of Figure 1a) is

$$\frac{\mathrm{d}}{\mathrm{d}r}\left(r\frac{\mathrm{d}\varphi}{\mathrm{d}r}\right) = 0 \tag{6}$$

which gives $r\mathrm{d}\varphi/\mathrm{d}r = k_{II}$ and

$$\varphi(r) = \varphi_p + k_{II}\ln\frac{r}{R_\mathrm{p}} \tag{7}$$

where $k_{II} \equiv R_\mathrm{p}(\mathrm{d}\varphi/\mathrm{d}r)_{R_\mathrm{p}+} = (\varepsilon_I R_\mathrm{p}/\varepsilon_{II})(\mathrm{d}\varphi/\mathrm{d}r)_{R_\mathrm{p}-}$. From eq 7, the effective gate potential $\varphi_\mathrm{p} \equiv \varphi(R_\mathrm{p})$ is

$$\varphi(R_\mathrm{p}) = \varphi_G - \frac{\varepsilon_I R_\mathrm{p}}{\varepsilon_{II}}\left(\frac{\mathrm{d}\varphi}{\mathrm{d}r}\right)_{R_\mathrm{p}-}\ln\frac{R_\mathrm{p}+d}{R_\mathrm{p}} \tag{8}$$

Finally, using the potential distribution $\varphi(r)$, the relative increase $\Delta G \equiv G - G_0$ in the nanopore conductance that can be achieved by the external gating is

$$\Delta G/G_0 = (2/R_\mathrm{p}^2)\int_0^{R_\mathrm{p}}[\cosh\varphi - 1]r\,dr \tag{9}$$

where $G_0 = \pi R_p^2\kappa_0/L$ is the nanopore conductance at zero gate potential, which depends on the nanostructure (radius R_p and length L) and electrolyte solution (electrical conductivity κ_0) characteristics.

Results and Discussion

Figure 1b shows the effective gate potential φ_p and the potential at the pore center $\varphi(0)$. Figure 1c shows the relative increase $\Delta G/G_0$ of the nanopore conductance vs the applied gate potential φ_G. We have used $d = 3$ nm and $\varepsilon_I/\varepsilon_{II} = 8$ as the dielectric layer characteristics. The electrical potentials are normalized to RT/F ($\varphi = 4$ corresponds to 100 mV approximately at 293 K). Although the potentials of Figure 1b are relatively high, it is not necessary to include ion-size effects[36] in the model: the ionic concentration at the pore surface, which can be estimated as $c_0 \exp\varphi_\mathrm{p}$, does not reach unrealistic high values because of the low bulk solution concentration c_0. Indeed, $c_0 \exp\varphi_\mathrm{p} = 0.2$ M for $c_0 = 0.5$ mM and $\varphi_\mathrm{p} = 6$ (see Figure 1b). The numbers $\kappa_{Dw}R_\mathrm{p}$ in the curves of parts b and c of Figure 1 are the ratios between the pore radius and the Debye length. Debye lengths $1/\kappa_{Di}$ in the range 3−10 nm would correspond to electrolyte concentrations c_0 in the range 1−10 mM approximately. These would give nanopore radii in the range $R_\mathrm{p} = 2-20$ nm for the ratios in the curves. Note that low enough electrolyte concentrations are required for tuning externally the nanopore conductance (the Debye length quantifying the extension of the electrical double layer over the pore cross section should be at least of the order of the pore radius[32,33,37] to enhance the gate effect). Also, for the gating to be effective, the gate electrode should be close enough to the solution region of the nanopore. The insulating region is however necessary to ensure the capacitive coupling and avoid leakage currents.[30]

The results of parts b and c of Figure 1 allow estimating the gate potential, which is needed to modulate efficiently the conductance for each nanopore and electrolyte solution characteristics. The effective gate potential φ_p is significantly lower than the applied gate potential φ_G, in agreement with experiments.[26−30] On the contrary, the predicted increases of the nanopore conductance with the gating are significantly higher than those observed experimentally,[26−30] probably because of the relatively thin insulating layer thickness and low electrolyte concentrations assumed. This is shown in Figure 1c where the discontinuous curve has been obtained with $d = 9$ nm instead of the thickness $d = 3$ used in the continuous curves. Other effects that could explain the highly efficient conductance gating (compared to previous experimental results[26−30]) obtained are the relatively low values of the ratio $\varepsilon_I/\varepsilon_{II}$ considered here as well as the fact that we ignore that the gate insulating layer may not be neutral at zero potential, providing a nonzero surface charge, and then an additional potential shift, that should affect the conductance gating (we are grateful to an anonymous reviewer for these suggestions). Finally, other side effects not accounted for in the model are concentration polarization[29] and ion adsorption.[31] Despite these limitations, the results appear to indicate that significant gating of the nanopore conductance could still be possible (see Figure 1c) because of the relatively high surface charge densities achieved (see Figure 1d for the effective charge density σ obtained at different gate potentials with $c_0 = 1$ mM).

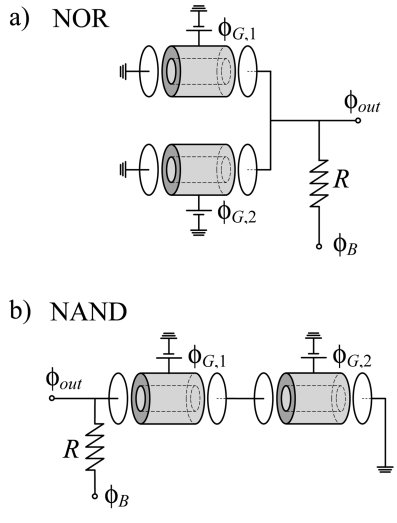

$\phi_{G,1}$/V	$\phi_{G,2}$/V	ϕ_{out}/V
0	0	0.83 (1)
1	0	0.09 (0)
0	1	0.09 (0)
1	1	0.05 (0)

$\phi_{G,1}$/V	$\phi_{G,2}$/V	ϕ_{out}/V
0	0	0.95 (1)
1	0	0.91 (1)
0	1	0.91 (1)
1	1	0.17 (0)

Figure 2. Schemes for the *NOR* (a) and *NAND* (b) logic gates obtained by gating the nanopore conductances at fixed bias potential $\phi_\mathrm{B} = 1$ V. The gate potentials ($i = 1, 2$) in the truth tables are the inputs, and the potential ϕ_out at the load resistance R is the output. Logic inputs (outputs) "1" and "0" correspond with high and low values of ϕ_{G_i} (ϕ_out), respectively. The nanopore and solution characteristics are $R_\mathrm{p} = 4.8$ nm, $L = 10$ μm, and $c_0 = 1$ mM.

Indeed, the gating efficiency depends critically on the effective surface charge density,[32] which determines the nanopore conductance G. Note also that $\sigma = 10\ \mu C/cm^2$ is equivalent to 0.6 e/nm^2 approximately, a typical surface charge density for nanopores,[15,20,32] where e is the elementary charge. This corresponds to an effective fixed charge concentration[36] $X = 2\sigma/(FR_p) = 200\ mM \gg 1\ mM = c_0$ for $R_p = 10$ nm. In this limit, the co-ion (the cation here) is virtually excluded from the pore,[32,36] and the assumption of total co-ion exclusion should be approximately valid. Therefore, it is the tuning of the counterion (the anion here) concentration in the pore by means of the gate potential that allows the gating of the nanopore conductance.

Figure 2 shows two schemes for the *NOR* (Figure 2a) and *NAND* (Figure 2b) logic gates that could be obtained by gating the nanopore conductances at fixed bias potential $\phi_B = 1$ V. The gate potentials ϕ_{G_i} ($i = 1, 2$) in the truth tables are the inputs, and the potential ϕ_{out} at the load resistance R is the output. Logic outputs "1" and "0" correspond to high and low values of ϕ_{out}, respectively. At high gate potentials (logic input "1") the nanopore is in the high-conducting state while at low gate potentials (logic input "0"), the opposite case occurs (see Figure 1c). We have assumed $R = 9 \times 10^{11}\ \Omega$, which is between the maximum and minimum values of $1/G$ that could be obtained in absence and presence of gating, respectively, and the following nanopore and solution characteristics: $R_p = 4.8$ nm, $L = 10\ \mu$m, and $c_0 = 1$ mM. In each case, the output voltage ϕ_{out} is obtained by solving the electrical circuit with the input values of the respective nanopore conductances (see Figure 1c).

The systems of Figure 2 constitute simple examples of circuits with more than one ionic element. Other nanofluidic architectures could now be used to implement a complete logic gate scheme[20] on the basis of the electrical gating of the nanopore conductance. Indeed, we have demonstrated theoretically and experimentally that single-track conical nanopores functionalized with polyprotic acid chains could also permit binary and multivalued logical functions because of the chemical tuning of the pH-sensitive fixed charges.[20] However, the experimental realization of the new scheme proposed here could avoid solution replacement and give faster time responses because the gating is electrical rather than chemical. Also, while the time response could be a limitation for nanofluidic diodes, this time could be decreased by several orders of magnitude using biological ion channels[19,35] and solid state synthetic nanopores,[2,38] whose thicknesses are of the order of 10 nm, instead of the relatively thick polymeric nanopores.

Conclusion

In conclusion, we have described how the *effective* gate potential at the insulating surface changes with the *applied* gate potential at the metallic surface. The results obtained allow us estimating the change in the nanopore conductance with the gate potential for different electrolyte concentrations and nanopore radii. The effective nanopore surface charge density that could be achieved in each experimental case has also been presented because this charge determines the nanopore selectivity in practical applications. Also, the experimental limitations making it difficult an effective modulation of the nanopore conductance have been emphasized in connection to parts b and c of Figure 1.

As a possible application, we have proposed logic gate schemes operating with electrical input and output signals based on the gating of the nanopore conductance (Figure 2). Because this gating can also be triggered by pore adsorption of charged chemical species from an external solution,[33] these logic schemes should also be of relevance for information processing in sensing applications.

Acknowledgment. We acknowledge the financial support from the Ministry of Science and Innovation of Spain, Materials Program (Project No. MAT2009-07747) and FEDER. Discussions with Prof. Zuzanna Siwy (UC Irvine) are also gratefully acknowledged.

References and Notes

(1) Siwy, Z.; Fuliński, A. *Phys. Rev. Lett.* **2002**, *89*, 198103.
(2) Dekker, C. *Nature Nanotechnol.* **2007**, *2*, 209.
(3) Ku, J. R.; Lai, S. M.; Ileri, N.; Ramirez, P.; Mafe, S.; Stroeve, P. *J. Phys. Chem. C* **2007**, *111*, 2965.
(4) Ali, M.; Yameen, B.; Neumann, R.; Ensinger, W.; Knoll, W.; Azzaroni, O. *J. Am. Chem. Soc.* **2008**, *130*, 16351.
(5) Healy, K.; Schiedt, B.; Morrison, A. P. *Nanomedicine* **2007**, *2*, 875.
(6) Murray, R. W. *Chem. Rev.* **2008**, *108*, 2688.
(7) Lee, S.; Zhang, Y. H.; White, H. S.; Harrell, C. C.; Martin, C. R. *Anal. Chem.* **2004**, *76*, 6108.
(8) Lebedev, K.; Mafe, S.; Stroeve, P. *J. Phys. Chem. B* **2005**, *109*, 14523.
(9) Zhang, Y. H.; Zhang, B.; White, H. S. *J. Phys. Chem. B* **2006**, *110*, 1768.
(10) Umehara, S.; Pourmand, N.; Webb, C. D.; Davis, R. W.; Yasuda, K.; Karhanek, M. *Nano Lett.* **2006**, *6*, 2486.
(11) Umehara, S.; Karhanek, M.; Davis, R. W.; Pourmand, N. *Proc. Natl. Acad. Sci. U.S.A.* **2009**, *106*, 4615.
(12) Siwy, Z.; Heins, E.; Harrell, C. C.; Kohli, P.; Martin, C. R. *J. Am. Chem. Soc.* **2004**, *126*, 10850.
(13) Vlassiouk, I.; Siwy, Z. *Nano Lett.* **2007**, *7*, 552.
(14) Kalman, E. B.; Vlassiouk, I.; Siwy, Z. *Adv. Mater.* **2008**, *20*, 293.
(15) Ali, M.; Ramirez, P.; Mafe, S.; Neumann, R.; Ensinger, W. *ACS Nano* **2009**, *3*, 603.
(16) Chun, K.-Y.; Mafe, S.; Ramirez, P.; Stroeve, P. *Chem. Phys. Lett.* **2006**, *418*, 561.
(17) Cheng, L.-J.; Guo, L. J. *ACS Nano* **2009**, *3*, 575.
(18) Ali, M.; Schiedt, B.; Healy, K.; Neumann, R.; Ensinger, W. *Nanotechnology* **2008**, *19*, 085713.
(19) Hille, B. *Ion channels of excitable membranes*; Sinauer Associates: Sunderland, MA, 2001.
(20) Ali, M.; Mafe, S.; Ramirez, P.; Neumann, R.; Ensinger, W. *Langmuir* **2009**, *25*, 11993.
(21) Pita, M.; Krämer, M.; Zhou, J.; Poghossian, A.; Schöning, M. J.; Fernandez, V. M.; Katz, E. *ACS Nano* **2008**, *2*, 2160.
(22) Ferreira, R.; Remon, P.; Pischel, U. *J. Phys. Chem. C* **2009**, *113*, 5805.
(23) Cervera, J.; Mafé, S. *Chem. Phys. Chem.* **2010**, *11*, 1654.
(24) Han, J.-H.; Kim, K. B.; Kim, H. C.; Chung, T. D. *Angew. Chem., Int. Ed.* **2009**, *48*, 3830.
(25) Zhan, W.; Crooks, R. M. *J. Am. Chem. Soc.* **2003**, *125*, 9934.
(26) Fan, R.; Yue, M.; Karnik, R.; Majumdar, A.; Yang, P. *Phys. Rev. Lett.* **2005**, *95*, 086607.
(27) Karnik, R.; Fan, R.; Yue, M.; Li, D.; Yang, P.; Majumdar, A. *Nano Lett.* **2005**, *5*, 943.
(28) Nam, S. W.; Rooks, M. J.; Kim, K. B.; Rossnagel, S. M. *Nano Lett.* **2009**, *9*, 2044.
(29) Kalman, E. B.; Sudre, O.; Vlassiouk, I.; Siwy, Z. *Anal. Bioanal. Chem.* **2009**, *394*, 413.
(30) Joshi, P.; Smolyanitsky, A.; Petrossian, L.; Goryll, M.; Saraniti, M.; Thornton, T. J. *J. Appl. Phys.* **2010**, *107*, 054701.
(31) Jing, Z.; Stein, D. *Langmuir* **2010**, *26*, 8161.
(32) Cervera, J.; Schiedt, B.; Neumann, R.; Mafe, S.; Ramirez, P. *J. Chem. Phys.* **2006**, *124*, 104706.
(33) Gao, X. P.; Zheng, G.; Lieber, C. M. *Nano Lett.* **2010**, *10*, 547.
(34) Stein, D.; Kruithof, M.; Dekker, C. *Phys. Rev. Lett.* **2004**, *93*, 03590.
(35) Alcaraz, A.; Ramirez, P.; Garcia-Gimenez, E.; Lopez, M. L.; Andrio, A.; Aguilella, V. M. *J. Phys. Chem. B* **2006**, *110*, 21205.
(36) Cervera, J.; Ramirez, P.; Manzanares, J. A.; Mafe, S. *Microfluid Nanofluid* **2010**, *9*, 41.
(37) Kontturi, K.; Murtomäki, L.; Manzanares, J. A. *Ionic Transport Processes*; Oxford University Press: Oxford, UK, 2008.
(38) Radenovic, A.; Trepagnier, E.; Csencsits, R.; Downing, K. H.; Liphardt, J. *Appl. Phys. Lett.* **2008**, *93*, 183101.

JP1087114